Environmental Modelling and Software 183 (2025) 106254

Contents lists available at ScienceDirect

Environmental Modelling and Software

journal homepage: www.elsevier.com/locate/envsoft

# An adaptable dead fuel moisture model for various fuel types and temporal scales tailored for wildfire danger assessment

Nicolò Perello[a,b,*], Andrea Trucchia[b], Mirko D'Andrea[b], Silvia Degli Esposti[b], Paolo Fiorucci[b], Andrea Gollini[c], Dario Negro[c]

[a] Department of Informatics, Bioengineering, Robotics and Systems Engineering, University of Genoa, via All'Opera Pia, 13, Genova, 16145, Italy
[b] CIMA Research Foundation, via A. Magliotto, 2, Savona, 17100, Italy
[c] Dipartimento della Protezione Civile, Presidenza del Consiglio dei Ministri, via Vitorchiano, 2, Roma, 00189, Italy

ARTICLE INFO

Dataset link: https://github.com/Perello-nico/DFMC_model, https://github.com/dvdkamp/fsmm

*Keywords:*
Dead fuel moisture content
Wildfires
Wildfire danger
Fire weather
Particle swarm optimization
Optimization

ABSTRACT

Estimating the Dead Fuel Moisture Content (DFMC) is crucial in wildfire risk management, representing a key component in forest fire danger rating systems and wildfire simulation models. DFMC fluctuates sub-daily and spatially, influenced by local weather and fuel characteristics. This necessitates models that provide sub-daily fuel moisture conditions for improving wildfire risk management. Many forest fire danger rating systems typically rely on daily fuel moisture models that overlook local fuel characteristics, with consequent impact on wildfire management. The semi-empirical parametric DFMC model proposed addresses these issues by providing hourly dead fuel moisture dynamics, with specific parameters to consider local fuel characteristics. A calibration framework is proposed by adopting Particle Swarm Optimization-type algorithm. In the present study, the calibration framework has been tested by using hourly 10-h fuel sticks measurements. Implementing this model in forest fire danger rating systems would enhance detail in forest fire danger conditions, advancing wildfire risk management.

## 1. Introduction

The estimation of fuel moisture content is a key factor in wildfire risk management, either in wildfire danger assessment and for fire-related land management practices, such as prescribed fire and agricultural burning (Silva et al., 2010, Matthews, 2014, Dragozi et al., 2021). In particular, Dead Fuel Moisture Content (DFMC i.e., moisture content of litter, dead grassland and dead woody debris) is of primarily importance, since it affects ignition likelihood and wildfire behavior in the first stages to a greater degree with respect to live fuel moisture (Silva et al., 2010, Matthews, 2014, Kang et al., 2023, Dragozi et al., 2021). For this reason, DFMC is typically considered in both Forest Fire Danger Rating (FFDR) systems (van Wagner, 1977, Nelson, 2000) and wildfire simulation models (Trucchia et al., 2020, Oliveira et al., 2023, Asensio et al., 2023). Dead fuel goes through drying and wetting phases during the day, involving complex processes that depend on local weather conditions, site and fuel characteristics (Matthews, 2014), making the topic still discussed in the literature (Bakšić and Bakšić, 2022, Shmuel et al., 2022 Hou et al., 2024, Fan et al., 2024, McNorton and Di Giuseppe, 2024).

DFMC can be measured both in-field methods, either by the collection and drying of fuel material, or by automatic instruments placed into the field (e.g., *fuel sticks*). However, the need to have spatially distributed information within the territory with next days forecast for wildfire management purposes has led to the use of models in operational routines (Matthews, 2014, Dragozi et al., 2021, Fan et al., 2024).

Different fuel moisture models have then been proposed in last decades, either *empirical* (van Wagner, 1977, Aguado et al., 2007, Lee et al., 2020, Fan and He, 2021, Shmuel et al., 2022, Bakšić and Bakšić, 2022) or *process-based* (Nelson, 2000, van der Kamp et al., 2017), within different frameworks and objectives — see the reviews of Viney (1991) and Matthews (2014) for more details. The present paper is focused on the use of DFMC models for wildfire danger assessment i.e., within FFDR systems.

* Corresponding author at: Department of Informatics, Bioengineering, Robotics and Systems Engineering, University of Genoa, via All'Opera Pia, 13, Genova, 16145, Italy.
*E-mail addresses:* nicolo.perello@edu.unige.it (N. Perello), andrea.trucchia@cimafoundation.org (A. Trucchia), mirko.dandrea@cimafoundation.org (M. D'Andrea), silvia.degliesposti@cimafoundation.org (S. Degli Esposti), paolo.fiorucci@cimafoundation.org (P. Fiorucci), Andrea.Gollini@protezionecivile.it (A. Gollini), Dario.Negro@protezionecivile.it (D. Negro).

https://doi.org/10.1016/j.envsoft.2024.106254
Received 24 July 2024; Received in revised form 21 October 2024; Accepted 24 October 2024
Available online 2 November 2024

Many FFDR systems rely on empirical or semi-empirical models, due to their limited information required and simple interpretation. As pointed out by Dragozi et al. (2021), accuracy, transferability, and simplicity of computation and interpretation are key features for a DFMC model to be used for operational purposes. In particular, these models are mainly based on weather information, allowing them to be computed on the basis of Numerical Weather Prediction models or automatic weather stations. As pointed out by Júnior et al. (2022), notable examples are represented by the Canadian Forest Fire Danger Rating System (CFFDRS; Lawson and Armitage, 2008) and the U.S. National Fire Danger Rating System (NFDRS; Carlson et al., 2007) - both of them include dedicated fuel moisture models. There are two aspects that are still discussed and source of interest in DFMC modeling for FFDR systems: the temporal resolution of the information provided, and the integration of fuel characteristics within the model.

Many models typically provide a daily description of the fuel moisture conditions. As an example, the Fire Weather Index (FWI) used by the CFFDRS, whose main dead fuel moisture sub-component is represented by the Fine Fuel Moisture Code (FFMC-FWI), is computed on daily basis at noon local time. Many authors pointed out the importance of considering a sub-daily fuel moisture dynamics to better describe fire danger changes during the day (Zhang and Sun, 2020, Lewis et al., 2024), and proposed consequently an adaptation of the FFMC-FWI index for hourly dynamics (van Wagner, 1977, Alexander et al., 1984, Bakšić et al., 2017). Also, new hourly fuel moisture indices have been proposed to this purpose (van der Kamp et al., 2017). The hourly FFMC-FWI dynamics will also be considered in the next generation of CFFDRS (Group, 2021), highlighting the need of an adaptation of the system to this aspect. Indeed, the sub-daily fuel moisture dynamics is of primarily importance in many regions of the World such as in the Mediterranean Basin, where rapid changes in relative humidity and temperature during the day can lead to high fire danger condition peaks within the day — see for example some case studies reported by Almeida et al. (2023).

The other important aspect in DFMC modeling regards the integration of fuel information within the model. Fuel type and understory characteristics are expected to influence fuel moisture dynamics (de Magalhães and Schwilk, 2021, Shmuel et al., 2022). The use of fuel type information can be of particular interest in areas where a high fuel variability is observed, such as the Mediterranean Basin. A classification is usually made in DFMC models according to fuel dimension or litter depth considered, due to the different response expected to weather conditions: the bigger the fuel or the deeper the litter layer, the slower the response rate is with respect to weather changes (Nelson, 2000). Fine fuels, such as dry grasses, needles, leaves or small branches, are of great interest in wildfire danger assessment because of their role in ignitions (Bakšić et al., 2017). They present rapid fuel moisture dynamics, leading to modification on wildfire danger on a hourly basis (Fiorucci et al., 2008). On the other hand, moisture conditions of larger fuels, such as dead tree logs in the understory or deeper litter layers, present a slower dynamics and they mainly affect the wildfire evolution in later stage after ignitions (van der Kamp et al., 2017). The fuel moisture dynamics can vary considerably in their response to weather conditions across the territory, depending on the fuel variability, with direct implications for wildfire danger assessment. DFMC models have typically addressed the issue either by using a proxy based on a reference fuel as *worst case* scenario, or by employing multiple indices, each corresponding to a different fuel class. The FFMC-FWI index, for example, has been developed and calibrated for a specific fine fuel type representative of the Canadian territory (i.e., pine needles). On the other hand, the NFDRS divides fuels with respect to their characteristic dimension, presenting then components for short and long-time response moisture dynamics in different indices.

A hybrid framework is used in the literature by the Italian Forest Fire Danger Rating System (RISICO; Fiorucci et al., 2008, 2011, 2018, Perello et al., 2022) adopted by the Italian Civil Protection Department for the issuance of the Daily National Forest Fire Forecast Bulletin. The development of RISICO started in the late '90 with an independent research from the CFFDRS and it is continuously updated in order to improve the capability to discriminate in space and time high risk areas. Prioritization is indeed crucial to implement sustainable and efficient prevention and preparedness strategies. Since the beginning in RISICO, the DFMC index differentiates its dynamics within the territory with the objective of discriminating fuel moisture dynamics among the most common type of fuels responsible for the ignition and propagation of wildfire such as, dry grasses, dry aerial fuels in shrubs and litters of conifers and broadleaves. For each fuel type, different saturation values and time lags have been considered. Indeed, it is reasonable to assume that moisture content in dry grasslands can rapidly change with rapid fluctuations in relative humidity, especially during strong winds. On the other hand, in deciduous forests, litter absorbs more moisture in case of rain and the release of moisture in the atmosphere is slower. Clearly, the moisture absorption and desorption processes in litter are more complex and would require additional data such as litter depth, density, and soil temperature, which cannot be measured at regional or national scales. Because of the complexity and heterogeneity of fuels, it may not be particularly useful from an operational perspective to develop different models for different fuels calibrated on local sampling. It is evident that even collecting long time series of hourly fuel moisture data coupled with meteorological data for different fuel type does not help to develop models able to represent the complexity of fuels, as their spatial heterogeneity prevents large-scale data collection. Nonetheless, the simple approach adopted in RISICO enabled to distinguish between rapid processes in fine fuels exposed to direct weather effects (such as dry aerial fuels in shrubs and dry grasslands) and slower processes in the litter. Although the development of this research initially began without knowledge of the Canadian model's structure, in the following years, the DFMC structure increasingly aligned with that of the Canadian model, but maintaining the original concept of differentiating between fuels. The ideas proposed in RISICO system have been used and extended in the model proposed in this paper.

In the present study, it is proposed a semi-empirical parametric DFMC model designed to simulate sub-daily fuel moisture dynamics, which can be calibrated to account for the characteristics of different local fuel types. A model calibration procedure is also proposed and tested over 10-h fuel sticks. The model and the calibration procedure proposed in this paper provide a complete framework for assessing sub-daily DFMC that can be adapted to different type of dead fuels. The structure of the paper is as follows: the next section describes the model, followed by the Material and Methods section in which the parametric calibration procedure is presented, together with the dataset utilized. The paper concludes with the presentation of the results, a discussion of the findings, and the final conclusions.

## 2. Dead fuel moisture content model

The main feature of the parametric model is its ability to simulate sub-daily fuel moisture dynamics, allowing for calibration based on time series observations of different fuel types. The model inputs are limited to near-surface weather conditions, namely temperature, relative humidity, wind speed and rain. As pointed out in Matthews (2014), also the solar radiation plays a role in drying process of fuels, with possible consequences for dead fuel in understory due to canopy shading effects. However, this effect has been often overlooked by DFMC models used in FFDR systems as for the FFMC-FWI, due also to the complexity in determining it for different canopy types and configurations on the ground. For this reason, it has not been considered as input in the present model, leaving this adaptation for future developments. In order to adapt the DFMC model to different type of dead fuel, two fuel-specific parameters are defined: the *saturation level* ($sat$, %) and the *standard response time* ($K_0$, $h$). Such parameters are related to fuel

**Table 1**
In the table, the list of variables used in the model is presented, together with unit of measurement and description.

| Variable | Unit | Description |
|---|---|---|
| $M_i$ | g | wet mass of fuel |
| $M_f$ | g | dry mass of fuel |
| DFMC | % | Dead Fuel Moisture Content with respect to $M_i$ |
| DFMC* | % | Dead Fuel Moisture Content with respect to $M_f$ |
| $\Delta$ | % | rain contribution to fuel moisture |
| $EMC$ | % | Equilibrium Moisture Content with respect to $M_i$ |
| $EMC^*$ | % | Equilibrium Moisture Content with respect to $M_f$ |
| K | h | fuel response time |
| $t$ | h | time |
| R | mm | cumulated rain |
| H | % | relative humidity |
| T | °C | air temperature |
| W | m/s | wind speed |
| sat | % | saturation level of fuel |
| $K_0$ | h | Standard Response Time of fuel |

characteristics and can be measured in standard conditions, without the need for long time series associated with meteorological variables as for the calibration of the other parameters. This aspect enhance the possibility of model calibration tests for different fuel types. To improve the clarity of the section, a list of variables used in this paragraph is presented in Table 1.

As done by Fiorucci et al. (2008), the fuel moisture content modeled here refers to the percentage of water content with respect to the total weight of fuel, computed as:

$$DFMC = 100\left(M_i - Mf\right)/Mi \tag{1}$$

where $M_i$ is the initial wet mass of fuel and $M_f$ is the dry mass of fuel, computed after drying process (from Silva et al., 2010). The use of this definition sets theoretically the fuel moisture values within 100%, which is many times preferred by end-users (Silva et al., 2010). However, many fuel moisture models in the literature refers to the water content with respect to the weight of fuel in dry conditions $DFMC^*$. The two quantities are related by the following map:

$$DFMC^* = 100DFMC/(100 - DFMC) \tag{2}$$

which allows the dynamics of fuel moisture to be transposed between the two definitions. A detailed discussion on this two fuel moisture definitions and moisture dynamics conversion is presented in the Appendix A.

As done by the FFMC-FWI, the proposed DFMC model distinguishes between two phases: a *rain phase* and a *no-rain phase*, depending on the rain occurred in the simulated time step. Since the model simulates sub-daily time steps, the two phases are considered mutually exclusive. Also, the model has been thought and calibrated for temperatures greater than 0 °C to avoid numerical issues. In case of negative temperatures, it is assumed that the model maintain fuel moisture conditions fixed (Fiorucci et al., 2008). Given the main use of the model in FFDR systems, this limitation has little impact on its use. Further generalizations of the model on this aspect will be considered in future studies.

### 2.1. Rain phase

If rain overcomes a threshold $\hat{R}$, the fuel moisture is increased:

$$DFMC = DFMC_0 + \Delta \tag{3}$$

with rapidity and magnitude depending both on rain occurred $R$ [mm] and distance from the saturation value $sat$ [%] following the structure of the FFMC-FWI:

$$\Delta = r_1 R \exp\left(-\frac{r_2}{sat - DFMC_0 + 1}\right)\left(1 - \exp\left(-\frac{r_3}{R}\right)\right) \tag{4}$$

$DFMC_0$ is the previous fuel moisture value and $r_1$, $r_2$, $r_3$ are model's parameters. The wetting process continue until the saturation value is reached, or rain stops. The rain threshold considers possible rain loss due to overhead canopy, as done by FFMC-FWI. The saturation value typically depends on fuel type (herbaceous fuel or small branches, fine fuel in conifers or broadleaves litter, etc., see examples in Matthews, 2014).

### 2.2. No-rain phase

In absence of rain, fuel moisture dynamics depends mainly on temperature, wind and relative humidity (Bakšić and Bakšić, 2022). In the presented model, the Byram's diffusion equation (Matthews, 2014) has been used:

$$DFMC^*(t) = EMC^* + \left(DFMC_0^* - EMC^*\right)\exp(-t/K) \tag{5}$$

defined for fuel moisture content obtained with respect to dry mass of fuel. The $DFMC_0^*$ is the initial fuel moisture value, $EMC^*$ is the *Equilibrium Moisture Content* [%] towards which the fuel moisture evolves, both defined with respect to dry conditions, and K is the *Response Time* [$h$] of the fuel. The explicit dependence on time allows the model to consider different time steps and so to simulate sub-daily dynamics.

By the use of the Formula (2), it is possible to derive the dynamics equation for the fuel moisture definition expressed by Formula (1) as adopted by the proposed model:

$$DFMC(t) = \frac{EMC - 100C\exp(-t/K)}{1 - C\exp(-t/K)}; \qquad C = \frac{EMC - DFMC_0}{100 - DFMC_0} \tag{6}$$

where $EMC$ and $DFMC_0$ are respectively the equilibrium moisture content and the initial fuel moisture condition with respect to wet mass of fuel, as defined by Formula (1). More details on the derivation of the previous equation can be found in Appendix A.

The fuel moisture dynamics in case of no-rain conditions shows an hysteresis behavior between the desorption and absorption of fuel moisture i.e., the *drying* and *wetting* processes. In the FFMC-FWI, this distinction is made both in the $EMC$ and the response time. However, the distinction in $EMC$ is usually ignored in many FFDR systems due to its little influence on the overall wildfire danger conditions (Fiorucci et al., 2008, Matthews, 2014). The proposed model differentiates the no-rain phase into *drying* and *wetting* sub-phases through a change in the response time, ignoring the $EMC$ contribution. The two sub-phases are identified according to the initial fuel moisture value with respect to $EMC$: if the initial moisture value is lower than the $EMC$, a wetting sub-phase occurs, and vice versa.

The EMC depends mainly on weather conditions, in particular relative humidity $H$ [%] and temperature $T$ [°C] (Matthews, 2014):

$$\begin{aligned} EMC(T,H) =& a_1 H^{a_2} + a_3\exp\left(\frac{H-100}{10}\right) + \\ &+ a_4(30 - \min(T,30))\left(1 - \exp\left(-a_5 H\right)\right) \end{aligned} \tag{7}$$

The equation has been adopted from FFMC-FWI, without considering different parameters values for drying and wetting sub-phase and adapting the contribution of air temperature to the Mediterranean environment.

The response time K is typically considered function of both fuel characteristics (as dimension, type, etc.) and weather conditions (Matthews, 2014, Bakšić et al., 2017), but its dependence is considered differently in the literature. In FFMC-FWI, K depends only on weather conditions: it is inversely proportional to wind and temperature, while it is directly proportional to humidity in drying phase and inversely proportional in wetting phase. In the NFDRS, K is mainly related to the fuel characteristics, dividing fuel types according to their dimension into 1-h, 10-h, 100-h, 1000-h response times — it is referred to standard weather conditions i.e., $T_{st}$ = 27 °C, $H_{st}$ = 20% and $W_{st}$ = 0 m/s (Nelson, 2000). In the DFMC model, a mixed formulation is proposed to incorporate both fuel characteristics and weather conditions i.e., temperature $T$ [°C], wind speed $W$ [m/s] and relative humidity $H$ [%]:

$$K_i(T, W, H) = K_0 G_i(T, W, H) \qquad i = d, w \tag{8}$$

where $i = d$ stands for *drying* and $i = w$ stands for *wetting*. The parameter $K_0$ refers to the *standard response time* $[h]$ in the standard weather conditions as defined by Nelson (2000), which is modified according to weather. To ensure the standard response time in standard conditions, the *dry/wet factor*:

$$G_i(T, W, H) = D_i g_i(T, W, H) \tag{9}$$

is normalized to 1 in the standard weather conditions by $D_i$, so that

$$K_i(T_{st}, W_{st}, H_{st}) = K_0$$

Different formulation for $g_i$ has been tested but keeping the goal of simplicity in the formulation (see the Supplementary Materials for the different formulations), and by selecting the one that performed better during the calibration process. Based on this analysis, the following formulation has been selected:

$$g_d = \frac{1 + b_{3,d} H^{c_{3,d}}}{1 + b_{1,d} T^{c_{1,d}} + b_{2,d} W^{c_{2,d}}} \qquad g_w = \frac{1 + b_{1,w} T^{c_{1,w}} + b_{2,w} W^{c_{2,w}}}{1 + b_{3,w} H^{c_{3,w}}} \tag{10}$$

In this formulation, the relative humidity favors the wetting process and reduces the time of absorption, while it increases the drying time; an opposite effect is instead expected for the wind and temperature contributions (Pausas and Keeley, 2021).

## 3. Material and methods

The following section is devoted to presenting the calibration framework. The dataset used for calibration and validation of the model's parameters is presented subsequently.

### 3.1. Calibration framework

The calibration framework can be summarized in the following steps, as described by Villaverde et al. (2022): formulation of the objective function; optimization algorithm; and goodness of fit analysis. The selection of the parameters to be calibrated is part of the application of the calibration framework. For this reason, the choice of model's parameters for the calibration performed in this paper is discussed in a separate paragraph in the Results section.

#### 3.1.1. Objective function

To calibrate the model's parameters, an optimization process has to be performed to minimize a specific objective function. In particular, the Sum of Squared Residuals function (SSR) (Villaverde et al., 2022) computed for the fuel moisture measurements has been selected:

$$f(\Theta) = \sum_{i=1}^{N} \sum_{k=1}^{T_i} \left( \hat{y}_i \left(t_k; \Theta, y_i \left(t_{k-1}\right), \mathbf{W}\left(t_k\right)\right) - y_i\left(t_k\right)\right)^2 \tag{11}$$

where $N$ is the number of time series used for calibration, $T_i$ is the number of time steps for time series $i$, $\hat{y}_i\left(t_k\right)$ and $y_i\left(t_k\right)$ are respectively the modeled and the observed fuel moisture value at time $t_k$ in the time series $i$. In the previous formula the model's output dependence on the weather conditions $\mathbf{W}$ at time $t_k$, and fuel moisture observations at time $t_{k-1}$ used as initial condition is made explicit. The optimization process then minimize the squared errors computed in a single time step of the model. The model's output depends on parameters vector $\Theta \in \mathbf{R}^n$, where $n$ is the dimension of the optimization problem i.e., the number of parameters to be calibrated. The minimization of $f(\Theta)$ over $\Theta$ is the objective of the optimization process, resulting in parameters calibration.

#### 3.1.2. Optimization algorithm

A meta-heuristic *Particle Swarm Optimization* (PSO) algorithm has been chosen for the optimization process. A PSO-type algorithm has been preferred since no particular regularity assumptions are required on the objective function, providing more flexibility with respect to other classic optimization algorithm. A PSO algorithm has been previously used in literature for a similar problem, see van der Kamp et al. (2017). In particular, the *Multi-Strategy Learning Particle Swarm Optimization* (MSL-PSO) has been adopted from Wang et al. (2021). The algorithm is a modification of the original PSO to deal with large dimension problems and reduce local minima drawback. For this reason, the MSL-PSO algorithm was preferred over the original PSO algorithm, after demonstrating better stability during preliminary testing. See Appendix B for more details in the algorithm adopted. The algorithm has been implemented in Python by the authors for its use in the calibration process. The code is made available in GitHub repository specified in the Software Availability section.

After the identification of the search space, whose identification depends on modeling choices during the application of the framework, different tests need to be performed to identify the number of particles and iterations, to ensure good parameters exploring and limit algorithm complexity. To further avoid local minima, the optimization algorithm can be performed for different calibration epochs, and selecting then the solution which results to the minimum objective function value on validation datasets. Also, the MSL-PSO algorithm presents two main hyper-parameters, namely the *number of probes* $p_{max}$ and the *social learning probability* $\phi$, which balance together the diversity and convergence capabilities of the algorithm — see Wang et al. (2021) and Appendix B for more details. Different tests on hyper-parameters choices can be performed, selecting then the hyper-parameters choice with the better performance on the validation datasets. Given the direct relation of $p_{max}$ with the algorithm computation cost, the number of probes has to be selected carefully.

#### 3.1.3. Goodness-of-fit analysis

Once the optimization process has been performed, different Goodness-of-Fit (GoF) measures can be used to assess model performances (Villaverde et al., 2022): the *Mean Absolute Error* (MAE), the *Bias*, the *Root Mean Square Error* (RMSE) and the *Normalized Nash–Sutcliffe Efficiency* (NNSE) (see Richter et al., 2011). The MAE corresponds to the average absolute difference between model and observations, while RMSE is an estimator of the standard errors deviations between model and observations — both are reported in data unit and are zero in case of complete agreement. The *Bias* is reported in data unit and it measures the mean deviation between model and observations: in case of positive bias, the model overestimate the observed values i.e., the model simulates wetter conditions, while a negative bias underestimate the observations, obtaining dryer values. Bias is zero in case of a perfect correspondence between model and observation. The NNSE is a dimensionless index in $[0, 1]$ derived by the *Nash–Sutcliffe Efficiency* (NSE) coefficient, which has been already used by van der Kamp et al. (2017) to assess fuel moisture model's performance. NNSE tests the model's ability to capture the observed variability. It is equal to 1 in case of perfect agreement between model and observation, while $NNSE = 0.5$ indicates that the model has the same predictive capability of the mean value of observation without adding much information on the dynamics of the simulated quantity.

### 3.2. Time series for calibration and validation

For the proposed model, the calibration dataset needs to consider both the time series collection of weather and fuel moisture conditions, representing respectively the model's inputs and output. Two different datasets have been involved in the calibration and validation process presented in this paper. The first dataset corresponds to fuel moisture measurements from five different sites collected by the Israel

Meteorological Service[1] and already used in literature by Shmuel et al. (2022) - hereafter this dataset is referred to as the *ISR dataset*. The data has been kindly shared by the authors of the mentioned paper. The second dataset corresponds to fuel moisture measurements from two different measurement tools located near Kamloops, British Columbia (Canada) and already used in literature by van der Kamp et al. (2017), whose authors made the data available through open-access repository[2] - hereafter this dataset is referred to as the *BC dataset*. In both the datasets `Campbell Scientific` CS506 Fuel Moisture Sensors were used to measure moisture levels of standard `Campbell Scientific 26601` 10-h Fuel Moisture Stick.[3] The 10-h fuel class refers to reference dowels of 0.65 cm radius and 50.8 cm length (van der Kamp et al., 2017, Carlson et al., 2007), following the fuel classification from the NFDRS. In the following, the measurement apparatus will be generically called *fuel stick*.

The use of the same measurement instrument allows the two datasets to be comparable and adopted in assessing the model performances, but testing the different location and conditions. The fuel moisture measurements are reported at hourly resolution, as average of 10 minutes records. Both the datasets present also the weather conditions measured every hour by weather stations close to the fuel sticks. The fuel moisture value recorded corresponds to the percentage of water content with respect to the stick weight in dry conditions, so measurements in both datasets have been then converted following the mapping of Formula (2) to make them compatible with the model's output. Let point out that the fuel moisture measurements of the fuel sticks present a known gap in values between 5% and 5.5% due to the conversion equation adopted to transform the pulse return time, measured from the sensor, into the fuel moisture content. Although the gap is in a range of values of particular interest for forest fire danger assessment, it does not compromise the overall calibration of the model.

The ISR dataset has been used for both the calibration and validation process, while the BC dataset has been used only for a further model validation. The two datasets are briefly described in the following paragraphs.

#### 3.2.1. ISR dataset

The five fuel sticks have been located in open areas with no canopy cover and close to meteorological stations. The five fuel sticks are located at different altitudes, spanning from 60 m to 936 m. Four fuel sticks measurements range from 2017 to 2021, while one fuel stick presents fuel moisture data from 2018. The time series present a good data continuity and completeness (Braca et al., 2013). The completeness is equal to 100% if all time steps are valid. The continuity is equal to 100% for a time series with all valid time steps and 0% for time series in which valid and invalid time steps alternates - a useful indication in case of calibration procedures. All the time series present a completeness almost over 70% and a continuity over 99%. More information on fuel sticks location and characteristics can be found in the Supplementary Materials.

The ISR dataset have been sampled and used for the calibration and validation process. In this study, a different approach was chosen compared to van der Kamp et al. (2017), where the model is calibrated separately on different time series. In particular, in this study shorter time series have been extracted from the different fuel sticks and mixed, to calibrate the model considering different conditions and enhance the diversity of the calibration dataset. Given the need to calibrate the two mutually exclusive model phases, two different samplings with specific characteristics have been performed: a *no-rain sampling* composed by 10 days time series without rain and a *rain sampling* composed by 6 hours time series with rain. The rain time series length has been limited due to the difficulty in obtaining continuous rain data, finding then a good threshold between representative of rain time series and sample size. Both the samplings have been performed to avoid *no data* time steps, and with temperatures greater than 0 °C to account for model's constraint on temperature. A third sampling called *mixed sampling* has been performed to assess the final calibrated model considering both rain and no-rain phases together. This sampling is composed by 10 days time series without any particular constraint on rain, with absence of no data time steps and with temperatures greater than 0 °C.

The sampling procedure used a semi-stochastic method: possible time intervals were identified given the constraints, and one was randomly selected. To avoid significant disruptions, an interval of the chosen length was taken from the first available time step, removed from the options, and the process repeated until no more intervals were available. The sampling procedure resulted to 274 no-rain time series, 350 rain time series and 408 mixed time series. Finally, the rain and no-rain samplings have been divided into calibration (80%) and validation (20%) datasets, resulting in: 220 and 54 time series respectively for calibration and validation of the no-rain phase; 280 and 70 time series respectively for calibration and validation of the rain phase. The mixed samplings have been used only for the model validation.

To better analyze model performances, the mixed samplings has been divided into two main clusters related to season: *Winter cluster* defined from November to April, and *Summer cluster* defined from May to October. The definition of the two seasons follows the typical division considered in the Mediterranean Winter and Summer fire seasons (Trucchia et al., 2022). The Winter cluster is composed by 186 time series, while Summer cluster is composed by 222 time series. The cluster definition has been guided by the need of assessing model performances in the two periods typically related with different fuel moisture conditions.

The variables distribution of the no-rain and rain samplings, and of the two clusters of the mixed samplings are reported in Fig. 1 - further analysis is available in the Supplementary Materials. The no-rain samplings present higher temperatures, and lower relative humidity values with respect to the rain samples, resulting in dryer fuel moisture conditions. This condition is also related to the higher density of no-rain samples in summer. For the mixed samplings, as expected by the clusters definition, the Winter cluster is associated with lower temperatures (mean value of 13 °C) and higher relative humidity (mean value of 70%) with respect to the Summer cluster, and presence of rain events, which translate in wetter fuel moisture conditions (mean value of 15%). On the other hand, the Summer cluster presents higher temperatures (mean value of 24 °C), lower relative humidity values (mean value of 60%) and typically few rain events, resulting into dryer fuel moisture conditions (mean value of 9%).

#### 3.2.2. BC dataset

The two fuel sticks are located in the same site, 639 m from each other, and in open areas with little or no canopy cover. The dataset is provided by van der Kamp et al. (2017) with completeness and continuity equal to 100%, and together with weather variables. The fuel moisture measurements were collected in Summer 2014, between May and September. In particular, one fuel stick (BC1) presents measurements from 2014/05/13 to 2014/09/21, while the other (BC2) presents measurements from 2014/06/05 to 2014/09/20. Further information on fuel sticks measurements can be found in van der Kamp et al. (2017). No particular information on latitude, longitude and altitude of the sites is provided by the author. The BC dataset has been used to assess model performance in different location with respect to the calibration dataset, and to test model performance in long time series. For this reason, the time series measurements of the BC dataset have been used without any sampling procedure. The variables distribution of the BC

[1] Israel Meteorological Service https://ims.gov.il/en (accessed: 06.05.2024)

[2] https://github.com/dvdkamp/fsmm?tab=readme-ov-file (accessed: 08.09.2024)

[3] The fuel stick characteristics are available at the website: https://www.campbellsci.com/pn26601

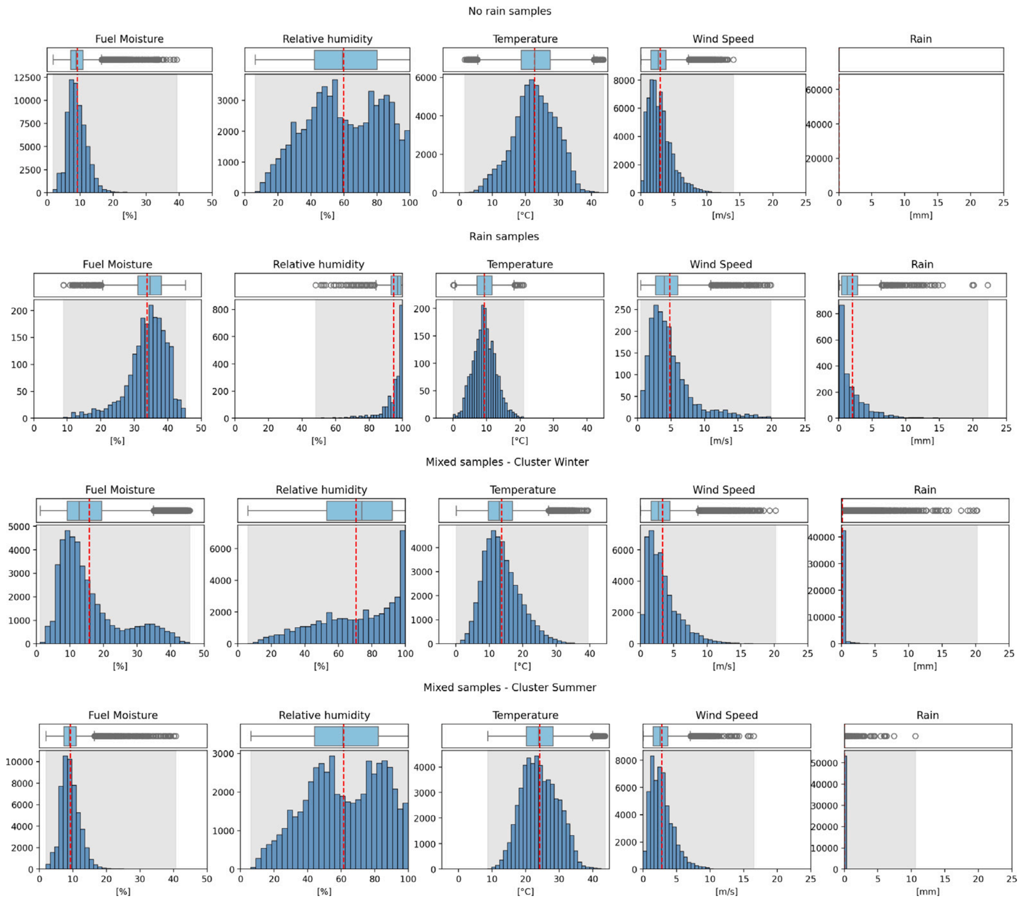


**Fig. 1. Time series samples statistics — ISR dataset.** In the figure, the distributions of the time series values from the no-rain, rain and mixed samplings of the Israel Meteorological Service dataset (ISR dataset) are reported — the mixed samplings are divided for the Winter and Summer clusters. The red dashed line represent the mean value of the variables, while the gray background enclose the range of variability.

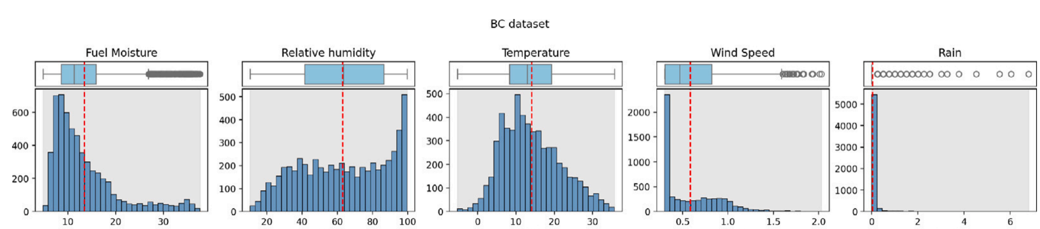


**Fig. 2. Time series samples statistics - BC dataset.** In the figure, the distributions of the time series values of the dataset provided by van der Kamp et al. (2017) (BC dataset) are reported. The red dashed line represent the mean value of the variables, while the gray background enclose the range of variability.

dataset is reported in Fig. 2 - further analysis is available in the Supplementary Materials. The BC dataset time series are characterized by few rain events, relative humidity mean value of 63% and temperature mean value of 14 °C. The fuel moisture mean value is around 13%, reaching minimum values around 5% and maximum of 38%.

## 4. Results

In the following section, the calibration settings and the results of the calibration process over the 10-h fuel sticks data are presented.

### *4.1. Calibration settings*

The rain and no-rain phases of the model were calibrated separately, given their mutual exclusivity, following the same procedure but on different samples of the dataset. In case of the rain phase, all the three parameters involved have been calibrated i.e., $r_1$, $r_2$ and $r_3$. For the no-rain phase, many parameters of the $EMC$ function are reported as used in the model adopted by RISICO, to limit the optimization problem dimension. Only parameter $a_1$ has been calibrated after its modification in the preliminary testing phase demonstrated an improvement in terms of model fitting performance. On the other hand, all the parameters of $K$ have been calibrated in the present study, corresponding to 12 parameters. Consequently, the no-rain phase calibration involved 13 parameters in total. The list of parameters is reported in Table 3. Let point out that parameters $D_d$ and $D_w$ are normalizing parameters, and so they are not involved in the calibration process but computed subsequently.

In the present study, the DFMC model has been calibrated with hourly fuel moisture measurements from 10-h fuel stick. For this reason, the fuel-dependent parameters $K_0$ and $sat$ have been set to 10 h and 45% respectively during the calibration process. Similar procedure can be adopted in case of calibration on different fuel types, setting the

**Table 2**
The table reports the Sum of Squared Residuals (SSR) values for the different hyper-parameter $\phi$ values used in the calibration of the rain and no-rain phases.

| | $\phi = 0.2$ | $\phi = 0.5$ | $\phi = 0.8$ |
|---|---|---|---|
| Rain phase | 1 136.9 | 1 136.9 | 1 136.8 |
| No-rain phase | 47 307.5 | 47 497.6 | 50 275.3 |

two fuel-specific parameters accordingly. The saturation value of 45% corresponds to the variability range of the fuel stick as reported in the manual of the 10-h fuel sticks used for calibration but converted to the fuel moisture scale of the DFMC model (see Eq. (2)).

For the rain phase, the parameters search space has been limited to [0.001, 80] for each parameter by following the variability range observed in RISICO equations, while for the no-rain phase different parameters search spaces are set according to the parameter considered: $a_1$ in [0.01, 1], $b_i$ in [0.1, 0.5] and $c_i$ in [0.5, 1]. The domain's limits have been identified following preliminary tests on calibration dataset to identify acceptable variability ranges of the quantities involved. In particular, the limits on parameters $b_i$ and $c_i$ have been identified to limit the increase of the standard response time, avoiding non-physical behaviors.

A population of 80 particles and 40 iterations have been considered, increasing swarm size with respect to the work done in van der Kamp et al. (2017) to improve the performance of the search process. The optimization algorithm has been repeated for 10 calibration epochs. All the epochs have been initialized using the *Latin Hypercube Sampling* method (McKay et al., 1979). Given the direct relation of $p_{max}$ with the algorithm computation cost, the number of probes has been fixed to 3 after some preliminary tests and following the work of Wang et al. (2021). However, different tests for $\phi = 0.2, 0.5, 0.8$ have been performed, selecting then the model parameters with the better performance on the validation datasets in terms of SSR function.

The optimization algorithm required almost 1700 s for the rain phase calibration, and almost 4700 s for the no-rain phase calibration — see Software Availability section for the details of the experimental environment in which the optimization algorithm has been performed.

The GoF measures have been computed separately for each time series of validation datasets, running the model on each time series starting from the first observed value and then letting proceed independently from observations. Given the presence of a transient during the no-rain phase, the GoF measures in the validation dataset for the no-rain phase and for the mixed samplings were evaluated starting from 72 h after the beginning of the time series.

### 4.2. Calibration results

The values of the SSR function for the different tests are reported in Table 2: for the rain phase, parameters obtained with $\phi = 0.8$ have been selected; for the no-rain phase, the parameters obtained with $\phi = 0.2$ have been chosen.

The calibrated parameters of the final DFMC model are reported in Table 3, while the different functions involved in the DFMC model as obtained from the calibration process are reported in Fig. 3.

In Fig. 4, the comparison between observed and simulated fuel moisture values for the mixed samplings of ISR dataset (Fig. 4a) and for the BC dataset (Fig. 4b) are reported, differentiating by colors between the two Summer and Winter clusters for the ISR dataset, and between the two fuel sticks $BC1$ and $BC2$ of the BC dataset.

The whole time series obtained from BC dataset are also reported in Fig. 5, together with the simulated response time and all the weather variables. The time series present few time steps with below-zero degree temperatures, where the fuel moisture value is maintained fixed according to the model definition — given the little occurrence of these conditions (see Fig. 5), it is not expected to alter significantly the results.

**Table 3**
The table contains the model's parameters.

| Phase | Parameter | Value |
|---|---|---|
| Rain phase | $r_1$ | 68.658964 |
| | $r_2$ | 53.374067 |
| | $r_3$ | 0.935953 |
| No-rain phase: EMC | $a_1$ | 0.5928 |
| | $a_2$ | 0.555 |
| | $a_3$ | 10.6 |
| | $a_4$ | 0.5022 |
| | $a_5$ | 0.0133 |
| No-rain phase: $K_d$ | $D_d$ | 1.082815 |
| | $b_{1,d}$ | 0.112756 |
| | $c_{1,d}$ | 0.531471 |
| | $b_{2,d}$ | 0.34982 |
| | $c_{2,d}$ | 0.534400 |
| | $b_{3,d}$ | 0.111055 |
| | $c_{3,d}$ | 0.517728 |
| No-rain phase: $K_w$ | $D_w$ | 0.931978 |
| | $b_{1,w}$ | 0.104363 |
| | $c_{1,w}$ | 0.509857 |
| | $b_{2,w}$ | 0.482954 |
| | $c_{2,w}$ | 0.6789 |
| | $b_{3,w}$ | 0.100061 |
| | $c_{3,w}$ | 0.504871 |

**Table 4**
The table presents the statistics (median, minimum, and maximum) of the Goodness-of-Fit (GoF) measures for the different mixed samplings from the Israel Meteorological Service dataset (ISR dataset), and the GoF measures for the time series from the dataset provided by van der Kamp et al. (2017) (BC dataset).

| | ISR dataset (median-min–max) *Mixed samplings* | | | BC dataset | |
|---|---|---|---|---|---|
| | Tot | Summer | Winter | *BC1* | *BC2* |
| MAE [%] | 1.84<br>0.47<br>7.22 | 1.49<br>0.48<br>4.23 | 2.60<br>0.47<br>7.22 | 2.46 | 2.25 |
| BIAS [%] | −0.02<br>−6.25<br>7.22 | −0.73<br>−4.17<br>4.12 | 0.83<br>−6.25<br>7.22 | 1.98 | 1.39 |
| RMSE [%] | 2.29<br>0.54<br>7.64 | 1.77<br>0.64<br>5.35 | 3.28<br>0.54<br>7.64 | 2.99 | 2.81 |
| NNSE [$adim$] | 0.65<br>0.06<br>0.98 | 0.56<br>0.06<br>0.93 | 0.79<br>0.11<br>0.98 | 0.85 | 0.85 |

The Goodness-of-Fit values computed for the validation datasets are reported in Table 4. In particular, the GoF measures are computed separately for each time series of the ISR dataset mixed samplings, and for the whole time series of the BC dataset. For the ISR dataset samplings, the median, minimum and maximum values are reported in the Table. The results are reported also for each cluster separately. The GoF measures for the rain and no-rain sampling validation datasets are reported in the Supplementary Materials.

The GoF measures computed for the mixed samplings of the ISR dataset are also reported in Fig. 6, where each matrix correspond to a different GoF measure, and each cell of the matrices corresponds to a different time series. The two clusters are highlighted with a label reported in each cell (namely, $S$ and $W$ respectively for Summer and Winter clusters). The same matrices are reported for the no-rain and rain samples validation datasets in the Supplementary Materials.

On the mixed samplings, the model presents a median MAE of 1.84%, showing then a quite good overall performance of the model given the fuel moisture range in [0%, 45%]. It presents also a median negative Bias of −0.02% reflecting a tendency in underestimation of fuel moisture values i.e., it simulates dryer conditions. Looking at the different clusters separately, the DFMC model performs slightly better on Summer cluster, where lower MAE and RMSE values (median

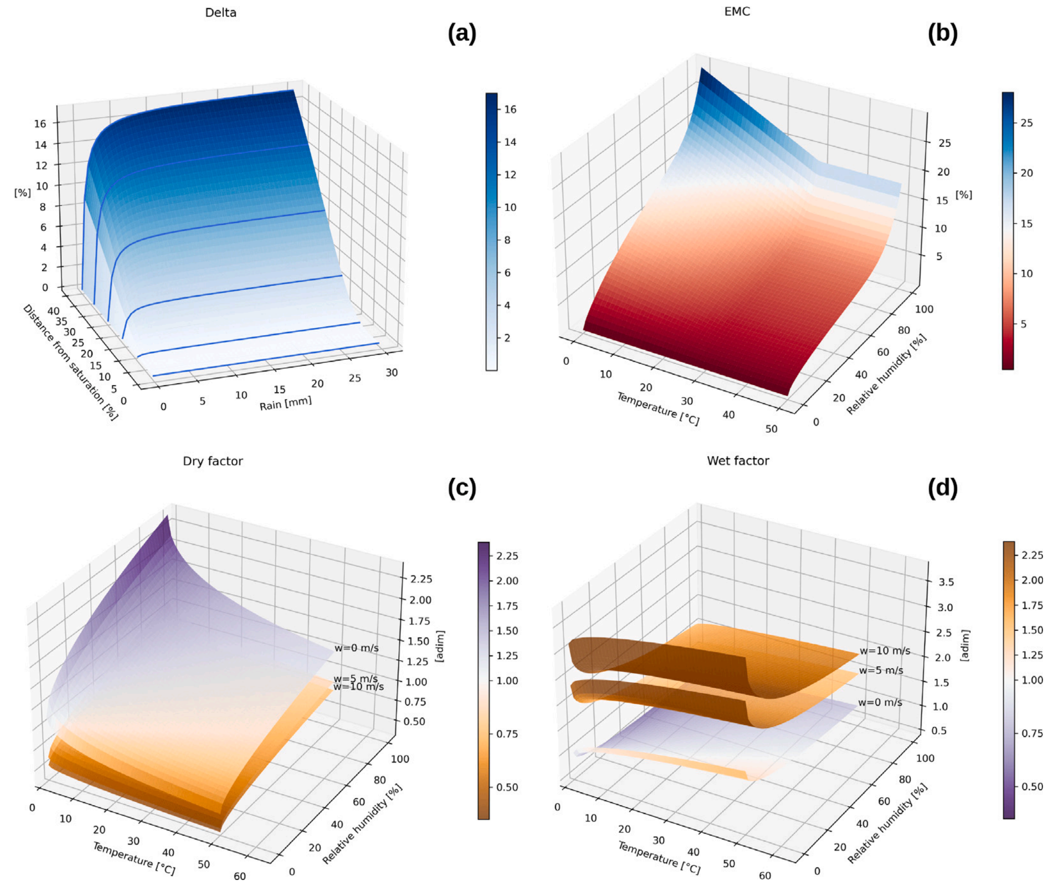


**Fig. 3. DFMC model's functions.** The figure displays the various functions that constitute the model, as obtained from its calibration: (a) the increase in fuel moisture due to rain, according to the distance of fuel moisture from saturation; (b) the Equilibrium Moisture Content, which depends on temperature and relative humidity; the dry (c) and wet (d) factor of the response time in the no-rain phase depending on temperature and relative humidity and for different wind speed values (the yellow color indicates conditions where drying process is favored, while purple color indicates conditions where wetting process is favored).

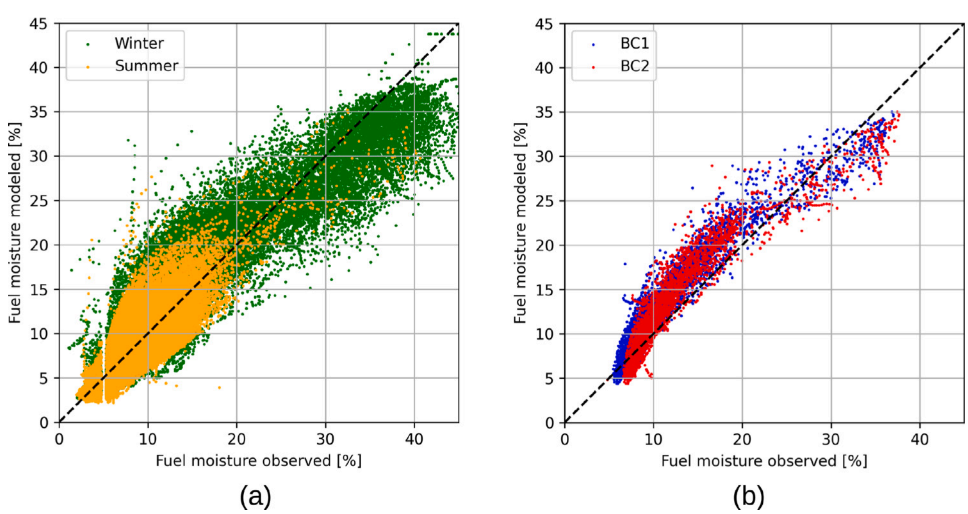


**Fig. 4. Observed vs. modeled fuel moisture.** The figure shows the comparison between observed and modeled fuel moisture values for: (a) the time series from the mixed samplings obtained from the Israel Meteorological Service dataset (ISR dataset); (b) the time series from the dataset provided by van der Kamp et al. (2017) (BC dataset). For the ISR dataset values, the points are colored based on their belonging to each cluster: two clusters are considered, namely Winter (in green) and Summer (in yellow). For the BC dataset values, the points are colored based on the two time series used: BC1 in blue, BC2 in red.

values respectively of 1.49% and 1.77%) and typically negative Bias values (median value of −0.73%) are obtained. On the other hand, Winter cluster presents higher MAE and RMSE values (median values respectively of 2.6% and 3.28%) and positive Bias (median value of 0.83%). Regarding the NNSE, Summer cluster shows smaller values (median value of 0.56) with respect to Winter cluster (median value of 0.79). Given the already low variability of fuel moisture values in Summer cluster due to the persistence of dry conditions, lower NNSE values are expected with respect to Winter cluster, where the presence of rain events also reflects in greater fuel moisture variability.

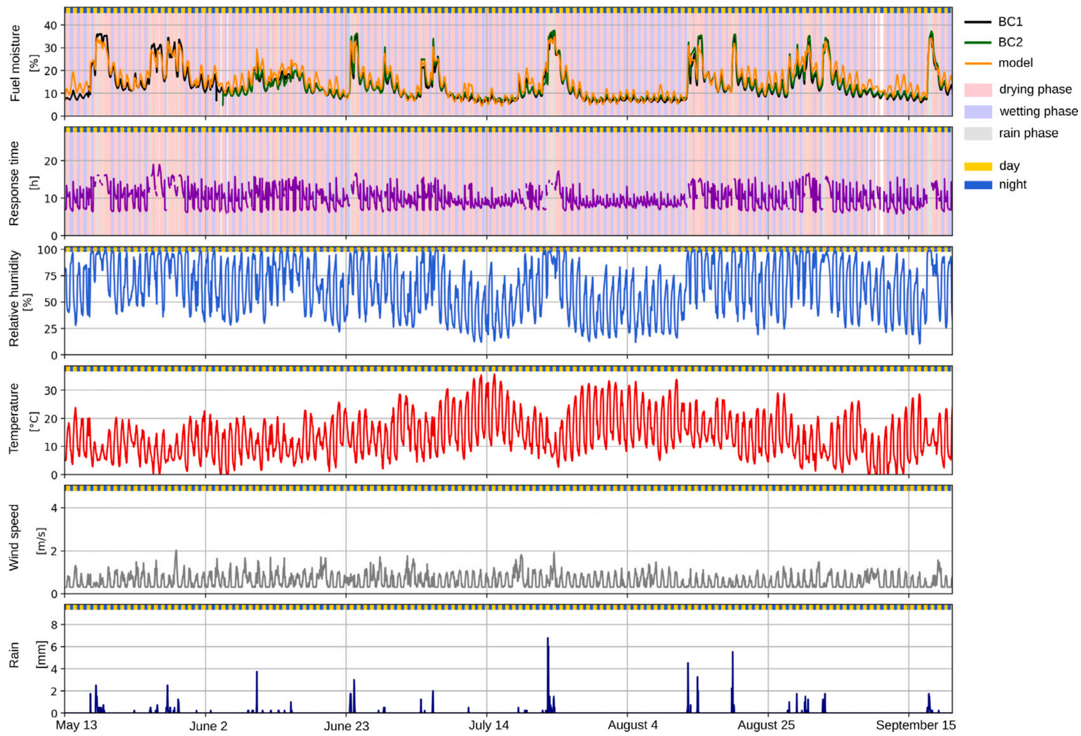


**Fig. 5. BC time series simulation.** The figure presents the two time series from the dataset provided by van der Kamp et al. (2017), along with their model simulations, the response time obtained from the model, and the input meteorological variables. The alternation of rain and no-rain phases is highlighted, with the latter further divided into drying or wetting phases. Also, the alternation of day (in yellow) and night (in blue) is highlighted in the upper part of each subplot.

Some examples of simulated time series from the mixed samplings are reported in Supplementary Materials. In the BC dataset, the model shows a MAE of around 2.25–2.46%, which is compatible with the fuel moisture range, and a slightly positive bias of 1.39–1.98%, while NNSE values over 0.85 identify a good ability of the model in describing fuel moisture variability during long time series.

## 5. Discussion

The DFMC model has been formulated to describe the sub-daily dynamics of fuel moisture, taking into account various possible fuel classes through a limited number of fuel-specific parameters, namely the saturation level and the standard response time. The definition of these two parameters is independent of the calibration itself, as they are characteristics of the fuel that can be measured separately. A procedure for calibrating the other model's parameters for different fuel types has been described and applied to a dataset of 10-h fuel stick data that can be representative of generic dead fuel having 10 h response time. This fuel type is considered of great interest in the literature for wildfire danger assessment, due to its direct role in the first stages of wildfires (Nelson, 2000, van Wagner, 1977, Shmuel et al., 2022). For this reason, 10-h fuel sticks are commonly used in many wildfire risk management systems worldwide, (Silva et al., 2010), given also the possibility of obtaining real-time measurements through *ad-hoc* remote sensors network — see for example the fire weather oriented Remote Automated Weather Stations in U.S..[4] Although it is known that fuel sticks measurements could be subject to errors (Matthews, 2014), the possibility of having hourly data coupled with weather conditions needed for model's calibration, guided the choice of the datasets used. While the dataset used can be considered sufficiently large for calibration, it covers a limited period and location. To our knowledge, extensive dead fuel moisture datasets with accompanying weather data are not yet widely available for regions of interest in wildfire research like the Mediterranean Basin. The ISR dataset used here, and referenced in prior studies, offers a valuable example. Further tests of the calibration process for different types of fuels and with different sampling procedures may be evaluated in future studies, based on the availability of similar datasets.

To evaluate its performance, the model has been used to simulate both mixed samplings from the ISR dataset, thus in conditions similar to those used for model calibration, and on the BC dataset to test its performance in different conditions and on long-term time series. The model demonstrated good performance, comparable to other studies (Aguado et al., 2007, Anderson and Anderson, 2009, van der Kamp et al., 2017, Bakšić et al., 2017), and acceptable for the model's objective of supporting wildfire danger assessment. In the mentioned studies, the MAE values are typically around 2–3%, comparable with the results obtained in the present study.

The performance analysis conducted separately for summer and winter conditions in the mixed samplings was driven by the need to evaluate the model in two scenarios typically associated with different fuel moisture conditions, and consequently with different fire danger conditions. The DFMC model shows better performance in the Summer cluster, with typical negative Bias values. It refers to time series in Summer period and low fuel moisture values, which are typically associated to higher wildfire danger conditions. Given the final purpose of the model to be used in Forest Fire Danger Rating systems, a negative bias in this conditions can be accepted as *worst case* scenario. Also, a better performance of the model in such conditions is desired, as observed in the MAE values obtained. On the other hand, the model shows slightly worse performance in Winter cluster, with positive Bias. These time series are associated with Winter season when high relative humidity and rain events are observed. The model shows then a degradation of performances in case of wetter fuel moisture conditions, typically when rain events are present and high relative humidity values are observed. This result can be observed also from the comparison between

[4] https://www.nifc.gov/about-us/what-is-nifc/remote-automatic-weather-stations, accessed: 2024-06-26

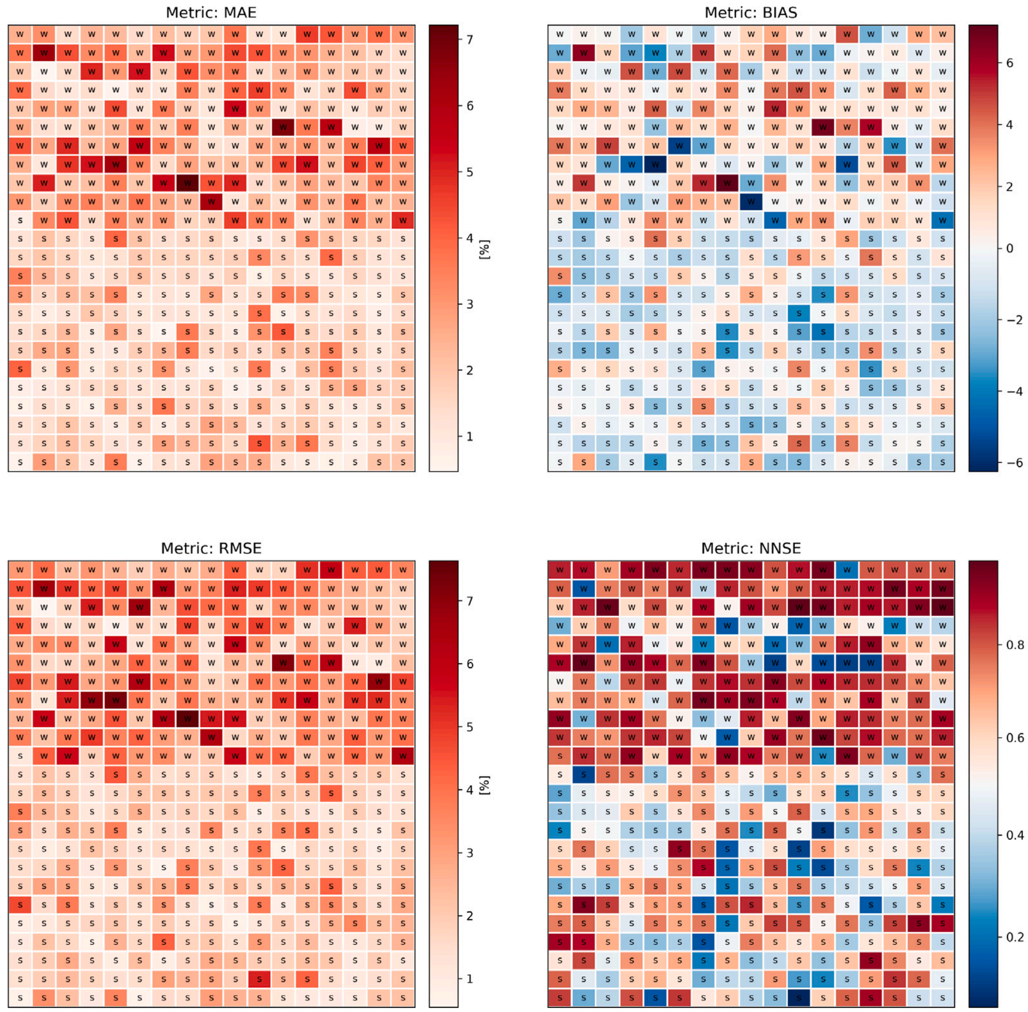


**Fig. 6. Goodness-of-Fit measures.** The matrices of the Goodness-of-Fit measures (MAE, Bias, RMSE, NNSE) obtained for the mixed samplings of the ISR dataset. Specifically, each cell in each matrix corresponds to a different time series. The two clusters, winter and summer, are highlighted with labels *W* and *S*, respectively.

observed and simulated fuel moisture in Fig. 4 where a degradation of performance is highlighted by the distortion in the plot for wetter fuel moisture conditions. The effect of rain events and the absorption of liquid water by fuel is a complex process in which local conditions and fuel characteristics are involved. The rain effect on the fuel wetting process still represents matter of discussion in the literature (Matthews, 2014). For this reason, empirical and simple process-based models have been typically adopted for wildfire danger assessment, as the one presented in this paper. However, given the complexity of the absorption process during rainfall, the use of an empirical model may lead to a poor description of the process, resulting in degraded performance. Additionally, focusing the calibration on more fire-prone conditions, in line with the model's objectives, may have introduced a bias towards low relative humidity conditions, leading to a degradation in performance when dealing with high relative humidity values. Given the final purpose of providing a fuel moisture model for wildfire danger conditions assessment, a degradation of performances in case of wetter conditions and rain events could have a limited impact. Nevertheless, in order to limit the under/over-estimation of fire danger conditions, especially during Winter seasons, an improvement of the model in the rain phase and for high relative humidity conditions is advocated in future studies. Another important aspect to be considered in future developments of the model, to improve its performance during the winter season, involves a specific adaptation for negative temperatures. Again, this aspect is still limited in the literature and could represent an area for improvement, especially for the use of the model in fire danger assessment in regions associated with winter fire regime.

Finally, the model showed a good performance in the long-term time series of the BC dataset, with results comparable with the ones obtained by van der Kamp et al. (2017) where RMSE values obtained are equal to 3.19% and 2.86% respectively for BC1 and BC2, and bias values equal to −0.38% and −0.09%, respectively. The model obtained by van Wagner (1977) showed negative bias, while positive bias was obtained for the DFMC model. This difference could be related to the different weather conditions observed in the BC dataset with respect to the ISR calibration dataset. In fact, the BC dataset conditions can be associated to the winter cluster of the mixed samplings (see Figs. 1 and 2), where positive bias is observed. As previously highlighted, these aspects warrant a thorough analysis and potential improvement of the model, which is deferred for future studies.

The model has currently been implemented in the testing phase as a spatial time-variant index, available operationally for the Italian Civil Protection Department within the MyDewetra platform (http://www.mydewetra.org, Italian Civil Protection Department, CIMA Research Foundation (2014)). An example is shown in Fig. 7. The model is used to compute pixel-by-pixel fuel moisture conditions. It represents an example of the operational use of the model for wildfire danger assessment at national level. As illustrated in the figure, the model can distinguish specific dry fuel conditions from wet ones, enabling the identification of elevated fire danger scenarios. The model currently runs with 1-hour and 1-km resolutions, employing Numerical Weather

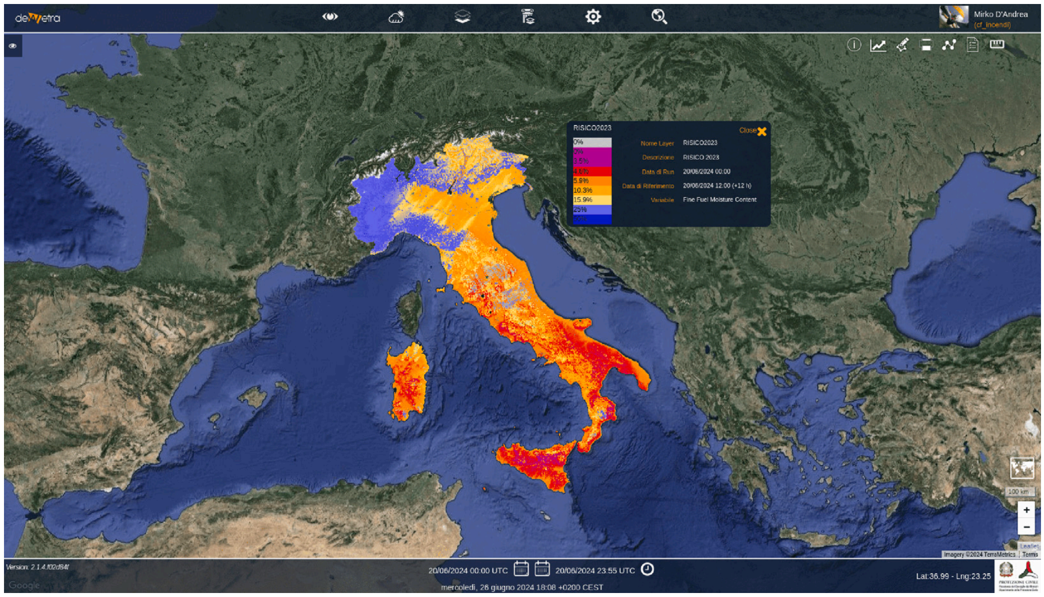


**Fig. 7. Example of operational implementation.** The figure displays the operational implementation of the fuel moisture model as index of the RISICO system, within the MyDewetra platform (http://www.mydewetra.org).

Predictions to forecast wildfire danger conditions for the next 3 days. The ability to obtain a next-days forecast of fuel moisture conditions supports better management of the wildfire risk system, allowing for the implementation of preparedness actions. The effectiveness of using the proposed DFMC model in wildfire danger assessment systems will be tested in future studies.

## 6. Conclusion

The estimation of Dead Fuel Moisture Content (DFMC) is essential for wildfire risk management. Currently, dead fuel moisture models used in the main Forest Fire Danger Rating systems provide daily information on fuel moisture, without considering the fuel on the territory, leading to a general overestimation of fire danger and losing the capability to identify local high danger condition in case of extreme weather conditions happen in the late afternoon or during night. More detailed information, with a higher sub-daily frequency, would improve wildfire risk management by identifying hours and areas of increased wildfire danger conditions.

This study has focused on the development and calibration of a semi-empirical parametric DFMC model to be used within Forest Fire Danger Rating systems, designed to simulate sub-daily moisture dynamics and to incorporate local fuel types characteristics. The principles of accuracy, transferability, and simplicity of computation and interpretation have been adopted in the design phase of the model. For this reason, the number of inputs needed are limited to weather conditions typically considered in both meteorological models and weather stations (i.e., temperature, relative humidity, wind speed and rain), while only two fuel-related parameters have been selected i.e., the standard response time and the saturation value.

A model's calibration framework has been also proposed. Calibration was performed using hourly 10-h fuel stick measurements, but in case of time series of specific dead fuel moisture are available, the proposed framework can be adopted to calibrate the model for other types of fuel. The DFMC model demonstrated good performance in validation datasets, with acceptable levels of Goodness-of-Fit measures. The model performs particularly well in conditions with low fuel moisture, related to high wildfire danger conditions, which is crucial for operational use of the model in wildfire danger assessment. There is, however, room for improvement in the model for the treatment of rain and wetter conditions.

The model successfully addresses the need for sub-daily fuel moisture dynamics, which is critical for accurate wildfire danger rating, particularly in regions with rapid changes in weather conditions. The possibility of integration of local fuel types enhances the model's applicability across different geographic regions, where high fuel heterogeneity is present, improving its adaptability and relevance. The DFMC model proposed provides a valuable tool for wildfire danger rating systems. By addressing the key aspects of temporal resolution and fuel characteristics, this model advances our capability to assess and respond to wildfire dangers effectively.

## Abbreviations

| Abbreviation | Description |
|---|---|
| BC dataset | Dataset of fuel sticks in British Columbia |
| CFFDRS | Canadian Forest Fire Danger Rating System |
| FFDR | Forest Fire Danger Rating |
| FFMC | Fine Fuel Moisture Content |
| FFMC-FWI | Fine Fuel Moisture Code module of the Fire Weather Index |
| FWI | Fire Weather Index |
| GoF | Goodness-of-Fit |
| ISR dataset | Dataset of fuel sticks from Israel Meteorological Service |
| MAE | Mean Absolute Error |
| MSL-PSO | Multi-Strategy Particle Swarm Optimization |
| NFDRS | U.S. National Fire Danger Rating System |
| NNSE | Normalized Nash–Sutcliffe Efficiency |
| PSO | Particle Swarm Optimization |
| RMSE | Root Mean Square Error |
| SSR | Sum of Squared Residuals |

## CRediT authorship contribution statement

**Nicolò Perello:** Writing – review & editing, Writing – original draft, Visualization, Validation, Software, Methodology, Formal analysis, Data curation, Conceptualization. **Andrea Trucchia:** Writing – review & editing, Methodology, Conceptualization. **Mirko D'Andrea:**

Methodology. **Silvia Degli Esposti:** Supervision. **Paolo Fiorucci:** Writing – review & editing, Supervision, Methodology, Conceptualization. **Andrea Gollini:** Supervision. **Dario Negro:** Supervision.

## Software availability

The codes that were used for the fuel moisture model calibration and assessment using Python language (version 3.11) can be found in GitHub: https://github.com/Perello-nico/DFMC_model, release $v1.0.0$. This repository was created by Nicolò Perello (E-mail: nicolo.perello@edu.unige.it) in October 2024 and has script files (almost 5 MB) and processed data (almost 12 MB). Author's experimental environment was as follows:

- OS: Ubuntu 23.04
- CPU: 13th Gen Intel®Core™i7-13700H ×20
- RAM: 32 GB
- GPU: Intel®Graphics (RPL-P)

## Declaration of competing interest

The authors declare that they have no known competing financial interests or personal relationships that could have appeared to influence the work reported in this paper.

## Acknowledgments

This research was funded by the Italian Civil Protection Department Presidency of the Council of Ministers, through the convention with CIMA Research Foundation, for the development of knowledge, methodologies, technologies, and training, useful for the implementation of national systems of monitoring, prevention, and surveillance.

## Appendix A. The two faces of the fuel moisture

The following paragraph presents two possible definitions of fuel moisture found in the literature (Silva et al., 2010), and their implications in describing fuel moisture dynamics.

The fuel moisture can be represented either as:

- the percentage of water content with respect to the total fuel weight, from now on referred to as $x$;
- the percentage of water content with respect to the fuel weight after drying process, from now on referred to as $x^*$.

The notation with $x$ and $x^*$ is made to simplify the notation of the following mathematical steps. The two quantities can be computed as follows:

$$x := 100\frac{M_i - M_f}{M_i} \tag{A.1}$$

$$x^* := 100\frac{M_i - M_f}{M_f} \tag{A.2}$$

where $M_i$ is the initial wet mass of fuel and $M_f$ is the dry fuel mass. Most of the research related to fuel moisture typically refers with respect to dry fuel i.e., $x^*$. However, many stakeholders use also the first definition since it is easier to interpret, being restricted theoretically to values within $[0, 100)$ unlike the $x^*$ definition in which $[0, +\infty)$ is the theoretical range. Let point out that the two ranges are defined as theoretical, since in both definition a saturation value is present, typically dependent on fuel types. The two definitions can be related by the following map:

$$\begin{aligned} &\varphi(x^*) : [0, +\infty) \longrightarrow [0, 100) \\ &\quad x = 100\left(\frac{x^*}{100 + x^*}\right) \end{aligned} \tag{A.3}$$

Given the presence of these two definitions, it is important to clarify their possible effects on the description of their dynamics, which is the focus of this section. In particular, the dynamics of fuel moisture as described by Byram's theory is analyzed, as it is widely used by many semi-empirical models (Matthews, 2014) such as the one presented in this paper.

Let start from the fuel moisture dynamics described by the following differential equation:

$$\begin{cases} K\dfrac{dx^*}{dt} + x^* = EMC^* \\ x^*(t=0) = x_0^* \end{cases} \tag{A.4}$$

The well-known solution corresponds to:

$$x^*(t) = EMC^* + (x_0^* - EMC^*)\exp(-t/K) \tag{A.5}$$

where $x_0^*$ is the initial condition and $EMC^*$ corresponds to the *Equilibrium Moisture Content* i.e, the fuel moisture value reached at equilibrium with external conditions — both the quantities are defined with respect to the dry fuel mass. The time required to reach the equilibrium condition is governed by the *response time* $K$, which is the time required to exchanged moisture equal to the $1 - e^{-1} \simeq 63\%$ of the difference between the initial and equilibrium moisture contents. The response time typically depends both on fuel characteristics and weather conditions, and it is independent on the fuel moisture definitions presented before.

The original equation has been derived for the fuel moisture computed as water content with respect to dry fuel i.e., $x^*$. However, given the previous equation, the fuel dynamics with respect to the total weight can be also derived.

Let assume fuel moisture dynamics $x^*(t)$ as known, then:

$$x(t) = \varphi(x^*(t)) \quad \forall t \tag{A.6}$$

It must be true, since it refers to the same physical quantity but in a different scale linked by the map $\varphi(\cdot)$. Let point out also that the initial condition and the equilibrium moisture content values must follow the same principle, so that $x_0 = \varphi(x_0^*)$ and $EMC = \varphi(EMC^*)$.

It is easy to demonstrate that the map $\varphi(\cdot)$ is $C^1$ (i.e., a continuous function with a continuous derivative) and it can be inverted, with $\varphi^{-1} \in C^1$:

$$\begin{aligned} &\varphi^{-1}(x) : [0, 100) \longrightarrow [0, +\infty) \\ &\quad x^* = 100\left(\frac{x}{100 - x}\right) \end{aligned} \tag{A.7}$$

Deriving the expression (A.6) with respect to $t$, we get:

$$\begin{aligned} \frac{dx}{dt} &= \frac{d}{dt}(\varphi(x^*)) = \frac{d\varphi}{dx^*}(x^*)\frac{dx^*}{dt} = \\ &= \frac{d\varphi}{dx^*}(x^*)\frac{1}{K}\left(EMC^* - x^*\right) = \\ &= \frac{d\varphi}{dx^*}(\varphi^{-1}(x))\frac{1}{K}\left(EMC^* - \frac{x}{100 - x}100\right) = \\ &= \frac{(100 - x)^2}{(100)^2}\frac{1}{K}\left(EMC^* - \frac{x}{100 - x}100\right) \end{aligned} \tag{A.8}$$

where the chain rule, the expression of $x^*(t)$ from Eq. (A.5) and the derivative theorem of the inverse function have been used. For the sake of notation, the time dependence of $x$ and $x^*$ is omitted. The previous expression can be manipulated to obtain:

$$(100)^2 K\frac{dx}{dt} = (100 - x)(100 + EMC^*)\left[100\frac{EMC^*}{100 + EMC^*} - x\right]$$

By noting that:

$$100 + EMC^* = 100 + \varphi^{-1}(EMC) = \frac{(100)^2}{100 - EMC}$$

and by using the definition of $EMC = \varphi(EMC^*)$, the differential equation for $x(t)$ dynamics can be obtained with all the fuel moisture values reported in the same scale of $x$:

$$\frac{dx}{dt} = \frac{1}{(100 - EMC)K}(100 - x)(EMC - x) \tag{A.9}$$

The solution of Eq. (A.9) can be easily obtained by integration:

$$x(t) = \frac{EMC - 100C\exp(-t/K)}{1 - C\exp(-t/K)} \tag{A.10}$$

where the constant $C$ can be found by imposing the initial condition $x(t = 0) = x_0$, so that:

$$C = \frac{EMC - x_0}{100 - x_0} \tag{A.11}$$

To conclude, Eq. (A.10) corresponds to the dynamics of fuel moisture according to Byram's theory but described as fuel moisture with respect to the total weight of fuel. The asymptotic behavior is that of convergence towards the stable equilibrium solution $EMC$, which corresponds to the equilibrium moisture content but expressed on the $x$-scale, as described by the Byram's theory. Let note that the same expression can be found by mapping Eq. (A.5) of $x^*$ dynamics directly through the map $\varphi(\cdot)$. The same procedure presented in this section can be used to derive the fuel moisture dynamics in different models according to the two definitions of fuel moisture proposed in the literature.

## Appendix B. The multi-strategy particle swarm optimization algorithm (MSL-PSO)

The balance between convergence and diversity within the population is a key aspect for meta-heuristic optimization algorithms to effectively address large-scale optimization problems (Wang et al., 2021). In fact, the exponential increase of the search space with the problem dimension pose a significant challenge in finding the global optimal solution. The Particle Swarm Optimization (PSO) algorithm show a quick convergence capability, but with the drawback of loosing the population diversity after some iterations i.e., after some generations of the population. This aspect affect the efficiency of the PSO algorithm in solving large-scale optimization problems, presenting the risk of finding local minima. Different modifications to the PSO algorithm has been proposed in literature, by adopting different learning strategy to improve the diversity of the population. The Multi-Strategy Particle Swarm Optimization Algorithm (MSL-PSO) proposed by Wang et al. (2021) is inspired by the *social learning PSO* proposed in Cheng and Jin (2015) in which each particle (an *imitator*) learn from some particles that have better fitness values (the *demonstrators*). In particular, in the MSL-PSO two different learning stages are proposed:

1. **Position probing**: each individual probe some positions by learning from its demonstrators who have better fitness values, and from the mean position of the population. The best probed position is then kept. All the best probes positions at current generation compose a temporary population, which inform the second learning stage;
2. **Position updating**: for each individual, two demonstrators are selected from the temporary population of best probed positions obtained in the first learning stage, and used to update the position.

The Algorithm 1 shows the pseudo-code of MSL-PSO, in which a population $Pop$ of $N$ individuals is generated and updated in position and velocity at each iteration of the algorithm until the *stop criterion* is reached. In the original paper of Wang et al. (2021), the stop criterion is made according to the number of evaluation of the objective function performed, which control the computational cost of the algorithm. In the present work, a maximum number of iterations is used as stop condition, along with checking if the iteration has made changes in the optimal solution with respect to the previous step, according to a predefined precision (i.e., $10^{-8}$ in the paper). In the Algorithm 1, $f$ denotes the objective function to be minimized, called *fitness*.

**Algorithm 1** The pseudocode of MSL-PSO

**Input:** Population size $N$;
**Output:** The optimal solution $\mathbf{x}_{best}$ and its fitness $f_{best}$;

Initialization of a population $Pop$;
Evaluate the fitness of each individual in $Pop$;
**while** *stop criterion* is False **do**
  Sort the population;
  **for** $i = 1 : N$ **do**
    Probe $p_{max}$ positions using the Algorithm 2 and keep the best solution among these $p_{\max}$ solutions;
  **end for**
  Evaluate the fitness of each individual in the new population $Pop^*$ composed by best positions probed for each individual in $Pop$;
  Sort the new population $Pop^*$;
  **for** $i = 1 : N$ **do**
    Find two sub-sets in the new population $Pop^*$ for the social learning of individual $i$, and update the population $Pop$ using Algorithm 3 - let be $\mathbf{x}_i(t+1)$ the updated position;
    Evaluate the new fitness value of individual $i$;
    **if** $f(\mathbf{x}_i(t+1)) < f(\mathbf{x}_{best})$ **then**
      $\mathbf{x}_{best} = \mathbf{x}_i(t+1)$;
      $f_{best} = f(\mathbf{x}_i(t+1))$;
    **end if**
  **end for**
  update *stop criterion*;
**end while**
Output the optimal solution and its fitness value.

*Position probing.* As first step, the current generation $Pop$ is sorted according to the fitness values, to identify the possible demonstrators of each particle i.e., all the individuals with greater ranking. For each individual, a maximum number $p_{max}$ of probes is performed. In particular, a different demonstrator $j$ is randomly selected for each dimension, and used to probe the positions of individual $i$ to ensure the diversity of probed positions, according to the following equations:

$$vv_{id}^k = r_1^k v_{id}(t) + r_2^k(x_{jd}(t) - x_{id}(t)) + \phi r_3^k(\bar{x}_d(t) - x_{id}(t)) \tag{B.1}$$

$$xx_{id}^k = x_{id}(t) + vv_{id}^k \tag{B.2}$$

where $d = 1, \dots, D$ denote the dimension selected among the possible $D$ dimensions, $k = 1, \dots, p_{max}$ is the probe index, $t$ is the generation index and $\bar{\mathbf{x}}(t) = \frac{1}{N}\sum_{i=1}^{N} x_i(t)$ is the mean position of population at generation $t$. The probed positions and velocity are then denoted by the vectors $\mathbf{xx}_i^k$ and $\mathbf{vv}_i^k$ respectively. The best probed position with minimum fitness value among the $p_{max}$ probed positions is kept for the second learning stage. Let us denote with $\mathbf{xc}_i$ the best probed position for individual i and with $\mathbf{vc}_i$ the corresponding velocity. At the end of the first stage, a second population $Pop^*$ is created, with the same number of individuals of the original population $Pop$ but composed by the best probing for each individual. $r_1^k$, $r_2^k$, $r_3^k$ are random numbers uniformly generated in $[0, 1]$. The parameter $\phi \in [0, 1]$ is called *social learning probability* and define the degree to learn from the mean position of population. The two hyper-parameters $p_{max}$ and $\phi$ control the diversity and convergence of the algorithm. The greater the number of probed positions, the more chance it will have to find the optimal solution at each iteration. However, it will greater computational costs. The social learning probability, on the other hand, controls how much the role of the demonstrators is considered with respect to the mean position of the population, influencing then the exploration of the search space.

**Algorithm 2** First learning stage: position probing

**Input:** individual $i$;
**Output:** the best probed position $\mathbf{xc}_i$;

**for** $k = 1 : p_{max}$ **do**
  **for** $d = 1 : D$ **do**
    Randomly select one individual from its demonstrators;
    Update the velocity on $d$th dimension using Eq. (B.1);
  **end for**
  Generate $k$th candidate position using Eq. (B.2);
**end for**
Evaluate the fitness values of these candidate positions;
$\mathbf{xc}_i = \arg\min\{f(\mathbf{xx}_1), f(\mathbf{xx}_2), \dots, f(\mathbf{xx}_{p_{\max}})\}$;

*Position updating.* Once the best probing population $Pop^*$ is provided, two demonstrators are selected from $Pop^*$ for each individual and used to update velocity and position according to the following equations:

$$v^k_{id}(t+1) = r_1 vc_{id} + r_2(xc_{jd} - xc_{id}) + \phi r_3(xc_{kd} - xc_{id}) \tag{B.3}$$

$$x_{id}(t+1) = xc_{id} + v_{id}(t+1) \tag{B.4}$$

where $\mathbf{vc}_i$ and $\mathbf{xc}_i$ are the velocity and position of the best probed position for individual i, while $j$ and $k$ represent the index of the two demonstrators $Dem_1$ and $Dem_2$ for individual $i$ to learn on dimension $d$. The selection of the two demonstrators is made according to the ranking of each individual and its probe. Let call $Rank(i)$ and $Rank^*(i)$ respectively the ranking of individual $i$ with position $\mathbf{x}_i$ in the original population $Pop$, and the ranking of the best probed position $\mathbf{xc}_i$ in population $Pop^*$. The first demonstrator $Dem_1$ is selected among the individuals of $Pop^*$ whose position stands between $Rank^*(i)$ and $Rank(i)$. If $Rank^*(i) < Rank(i)$ it means that the individual $i$ falls behind more other individuals in $Pop^*$ compared to $Pop$, so $Dem_1$ is selected until the position occupied in the original population $Pop$. On the other hand, if $Rank^*(i) > Rank(i)$, $Dem_1$ is selected among the losers in $Pop^*$ to prevent premature convergence. The second demonstrator $Dem_2$ is selected from all individuals that have better fitness than the best probed position. See Wang et al. (2021) for more details.

**Algorithm 3** Second learning stage: position updating

**Require:** the best probe position of individual $i$ ($\mathbf{xc}_i$);
**Ensure:** the position of individual $i$ at generation $t+1$;
**for** d=1:D **do**
  select demonstrator 1 $Dem_1$;
  select demonstrator 2 $Dem_2$;
  Update the velocity and position using Eqs. (B.3) and (B.4), respectively;
**end for**

As reported by Wang et al. (2021), the MSL-PSO algorithm performed well in solving large dimensional optimization problems with respect to the state of the art algorithms. The Authors of this paper implemented the algorithm in Python, and made available through public GitHub repository (see Section Software for more details).

## Appendix C. Supplementary data

Supplementary material related to this article can be found online at https://doi.org/10.1016/j.envsoft.2024.106254.

## Data availability

The data used for calibration and validation can be found in GitHub repository: https://github.com/Perello-nico/DFMC_model, release $v1.0.0$. The repository contains the time series obtained from the ISR dataset and BC dataset, which are described in the paper. The ISR dataset used for calibration and validation was kindly shared by the authors of Shmuel et al. (2022) under request. The BC dataset used for validation has been share by the authors of van der Kamp et al. (2017) through open GitHub repository (https://github.com/dvdkamp/fsmm).

## References


Aguado, I., Chuvieco, E., Borén, R., Nieto, H., 2007. Estimation of dead fuel moisture content from meteorological data in mediterranean areas. Applications in fire danger assessment. Int. J. Wildland Fire 16, 390–397. http://dx.doi.org/10.1071/WF06136.

Alexander, M.E., Lee, B., Lee, C.Y., 1984. Hourly calculation of the fine fuel moisture code, ISI and FWI with Texas instruments model 59 hand-held calculator (File Report NOR-5-19). Technical Report, Northern Forest Research Centre - Canadian Forestry Service, Edmonton.

Almeida, M., Ribeiro, L., Alves, D., Viegas, D., Vaz Pinto, V., Marques, R., Gomes, A., Ballereau, D., Lahaye, S., Romain, M., Salis, M., Arca, B., Bacciu, V., Canu, A., Del Giudice, L., Duce, P., Pellizzaro, G., Stroppiana, D., Ventura, A., Cabiddu, S., Casula, A., Cuccu, G., Pinna, T., Vaccargiu, M., Campesi, S., Casule, F., Chessa, M., Cinus, S., Massidda, P., Peddes, M., Soi, F., Tola, F., Usai, A., Castiglia, C., Dessy, C., Delitala, A., Trudu, P., Angotzi, S., Murtas, F., Barone, A., Erriu, N., Fresu, G., Melis, G., Fiorucci, P., Pampanoni, V., Laneve, G., Eftychidis, G., Varela, V., Gkotsis, I., Petrou, K., Boustras, G., Senekkis, I., Kirschner, J., Pandey, P., San-Miguel-Ayanz, J., Durrant, T., Libertà, G., Boca, R., Maianti, P., Branco, A., Jacome Felix Oom, D., De Rigo, D., Roglia, E., Scionti, N., Suarez-Moreno, M., 2023. Analysis of 2021 critical wildfire events in the Mediterranean region. Technical Report, Publications Office of the European Union, Luxembourg, http://dx.doi.org/10.2760/562495.

Anderson, S.A., Anderson, W.R., 2009. Predicting the elevated dead fine fuel moisture content in gorse (Ulex europaeus L.) shrub fuels. Can. J. Forest Res. 39 (12), 2355–2368. http://dx.doi.org/10.1139/X09-142.

Asensio, M., Cascón, J., Laiz, P., Prieto-Herráez, D., 2023. Validating the effect of fuel moisture content by a multivalued operator in a simplified physical fire spread model. Environ. Model. Softw. 164, 105710. http://dx.doi.org/10.1016/j.envsoft.2023.105710, URL https://www.sciencedirect.com/science/article/pii/S1364815223000968.

Bakšić, N., Bakšić, D., 2022. Equilibrium Moisture Content of Dead Fine Fuels of Pubescent Oak (Quercus pubescens Willd.) and Holm Oak (Quercus ilex L.). 17, (1), p. 42. http://dx.doi.org/10.3390/environsciproc2022017042.

Bakšić, N., Bakšić, D., Jazbec, A., 2017. Hourly fine fuel moisture model for Pinus halepensis (Mill.) litter. Agricult. Forest. Meterol. 243, 93–99. http://dx.doi.org/10.1016/j.agrformet.2017.04.014.

Braca, G., Bussettini, M., Lastoria, B., Mariani, S., 2013. Linee guida per l analisi ed elaborazione statistica di base delle serie storiche di dati idrologici. Technical Report, Istituto Superiore per la Protezione e Ricerca Ambientale (ISPRA) - Dipartimento Tutela delle Acque Interne e Marine – Servizio Monitoraggio e Idrologia delle Acque Interne – Settore Idrologia.

Carlson, J.D., Bradshaw, L.S., Nelson, R.M., Bensch, R.R., Jabrzemski, R., 2007. Application of the Nelson model to four timelag fuel classes using Oklahoma field observations: Model evaluation and comparison with National Fire Danger Rating System algorithms. Int. J. Wildland Fire 16 (2), 204–216. http://dx.doi.org/10.1071/WF06073.

Cheng, R., Jin, Y., 2015. A social learning particle swarm optimization algorithm for scalable optimization. Inform. Sci. 291, 43–60. http://dx.doi.org/10.1016/j.ins.2014.08.039.

de Magalhães, R.Q., Schwilk, D.W., 2021. Moisture absorption and drying alter nonadditive litter flammability in a mixed conifer forest. J. Ecol. 109, 234–245. http://dx.doi.org/10.1111/1365-2745.13467.

Dragozi, E., Giannaros, T.M., Kotroni, V., Lagouvardos, K., Koletsis, I., 2021. Dead fuel moisture content (Dfmc) estimation using modis and meteorological data: The case of Greece. Remote Sens. 13 (21), http://dx.doi.org/10.3390/rs13214224.

Fan, C., He, B., 2021. A physics-guided deep learning model for 10-h dead fuel moisture content estimation. Forests 12 (7), http://dx.doi.org/10.3390/f12070933.

Fan, C., He, B., Yin, J., Chen, R., Zhang, H., 2024. Process-based and geostationary meteorological satellite-enhanced dead fuel moisture content estimation. GISci. Remote Sens. 61 (1), 2324556. http://dx.doi.org/10.1080/15481603.2024.2324556.

Fiorucci, P., D'Andrea, M., Bastia, S., Gollini, A., Gualtieri, S., Negro, D., Severino, M., 2018. II Aggiornamento Del Manuale D'uso del Sistema Previsionale Della Pericolosità Potenziale Degli Incendi Boschivi RIS.I.CO. Technical Report, Italian Department of Civil Protection—Presidency of the Council of Ministers and CIMA Research Foundation, URL https://www.mydewetra.org/wiki/index.php/RISICO_2015.

Fiorucci, P., D'Andrea, M., Negro, D., Severino, M., 2011. Manuale d'uso del Sistema Previsionale della Pericolosità Potenziale Degli Incendi Boschivi RIS.I.CO. Technical Report, Italian Department of Civil Protection—Presidency of the Council of Ministers and CIMA Research Foundation.

Fiorucci, P., Gaetani, F., Minciardi, R., 2008. Development and application of a system for dynamic wildfire risk assessment in Italy. Environ. Modell. Softw. 23 (6), 690–702. http://dx.doi.org/10.1016/j.envsoft.2007.05.008.

Group, C.F.S.F.D., 2021. An overview of the next generation of the Canadian Forest Fire Danger Rating System (Information Report GLC-X-26). Technical Report, Natural Resources Canada, Canadian Forest Service, Great Lakes Forestry Centre, URL https://osdp-psdo.canada.ca/dp/en/search/metadata/NRCAN-CFS-1-40474. accessed: 2 July 2024.

Hou, X., Wu, Z., Zhu, S., Li, Z., Li, S., 2024. Comparative analysis of machine learning-based predictive models for fine dead fuel moisture of subtropical forest in China. Forests 15 (5), http://dx.doi.org/10.3390/f15050736.

Italian Civil Protection Department, CIMA Research Foundation, 2014. The dewetra platform: A multi-perspective architecture for risk management during emergencies. In: Hanachi, C., Bénaben, F., Charoy, F.c. (Eds.), Information Systems for Crisis Response and Management in Mediterranean Countries. Springer International Publishing, Cham, pp. 165–177.

Júnior, J.S., Paulo, J.R., Mendes, J., Alves, D., Ribeiro, L.M., Viegas, C., 2022. Automatic forest fire danger rating calibration: Exploring clustering techniques for regionally customizable fire danger classification. Expert Syst. Appl. 193, 116380. http://dx.doi.org/10.1016/j.eswa.2021.116380.

van der Kamp, D.W., Moore, R.D., McKendry, I.G., 2017. A model for simulating the moisture content of standardized fuel sticks of various sizes. Agricult. Forest. Meterol. 236, 123–134. http://dx.doi.org/10.1016/j.agrformet.2017.01.013.

Kang, Z., Quan, X., Lai, G., 2023. Assessing the Effects of Fuel Moisture Content on the 2018 Megafires in California. IEEE J. Sel. Top. Appl. Earth Obs. Remote Sens. 16, 868–877. http://dx.doi.org/10.1109/JSTARS.2022.3232665.

Lawson, B.D., Armitage, O.B., 2008. Weather Guide Canadian Forest Fire Danger Rating System. Canadian Forest Service Northern Forestry Centre. Canadian Forest Service, Norther Forestry Centre, pp. 1–73, URL https://cfs.nrcan.gc.ca/pubwarehouse/pdfs/29152.pdf. accessed 2 July 2024.

Lee, H.T., Won, M., Yoon, S., Jang, K., 2020. Estimation of 10-h fuel moisture content using meteorological data: A model inter-comparison study. Forests 11 (9), 1–19. http://dx.doi.org/10.3390/f11090982.

Lewis, C., Little, K., Graham, L.J., Kettridge, N., Ivison, K., 2024. Diurnal fuel moisture content variations of live and dead Calluna vegetation in a temperate peatland. Sci. Rep. 14 (1), http://dx.doi.org/10.1038/s41598-024-55322-z.

Matthews, S., 2014. Dead fuel moisture research: 1991–2012. Int. J. Wildland Fire 23 (1), 78–92. http://dx.doi.org/10.1071/WF13005.

McKay, M.D., Beckman, R.J., Conover, W.J., 1979. A comparison of three methods for selecting values of input variables in the analysis of output from a computer code. Technometrics 2 (2), 239–245. http://dx.doi.org/10.2307/1268522.

McNorton, J.R., Di Giuseppe, F., 2024. A global fuel characteristic model and dataset for wildfire prediction. Biogeosciences 21 (1), 279–300. http://dx.doi.org/10.5194/bg-21-279-2024.

Nelson, J., 2000. Prediction of diurnal change in 10-h fuel stick moisture content. Can. J. Forest Res. 30 (7), 1071–1087. http://dx.doi.org/10.1139/cjfr-30-7-1071.

Oliveira, U., Soares-Filho, B., Rodrigues, H., Figueira, D., Gomes, L., Leles, W., Berlinck, C., Morelli, F., Bustamante, M., Ometto, J., Miranda, H., 2023. A near real-time web-system for predicting fire spread across the cerrado biome. Sci. Rep. 13, http://dx.doi.org/10.1038/s41598-023-30560-9.

Pausas, J.G., Keeley, J.E., 2021. Wildfires and global change. Front. Ecol. Environ. 19, 387–395. http://dx.doi.org/10.1002/fee.2359.

Perello, N., Trucchia, A., D'Andrea, M., Degli Esposti, S., Fiorucci, P., 2022. RISICO, an enhanced forest fire danger rating system: Validation on 2021 extreme wildfire season in southern Italy. 17, (1), p. 37. http://dx.doi.org/10.3390/environsciproc2022017037,

Richter, K., Hank, T.B., Atzberger, C., Mauser, W., 2011. Goodness-of-fit measures: what do they tell about vegetation variable retrieval performance from earth observation data. In: Neale, C.M.U., Maltese, A. (Eds.), Remote Sensing for Agriculture, Ecosystems, and Hydrology XIII. In: Society of Photo-Optical Instrumentation Engineers (SPIE) Conference Series, vol. 8174, p. 81740R. http://dx.doi.org/10.1117/12.897980.

Shmuel, A., Ziv, Y., Heifetz, E., 2022. Machine-Learning-based evaluation of the time-lagged effect of meteorological factors on 10-h dead fuel moisture content. Forest Ecol. Manag. 505, 119897. http://dx.doi.org/10.1016/j.foreco.2021.119897.

Silva, J.S., Rego, R., Fernandes, P., Rigolot, E., 2010. Towards Integrated Fire Management – Outcomes of the European Project Fire Paradox. Technical Report, European Forest Institute.

Trucchia, A., D'Andrea, M., Baghino, F., Fiorucci, P., Ferraris, L., Negro, D., Gollini, A., Severino, M., 2020. PROPAGATOR: An operational cellular-automata based wildfire simulator. Fire 3 (3), http://dx.doi.org/10.3390/fire3030026, URL https://www.mdpi.com/2571-6255/3/3/26.

Trucchia, A., Meschi, G., Fiorucci, P., Gollini, A., Negro, D., 2022. Defining wildfire susceptibility maps in Italy for understanding seasonal wildfire regimes at the national level. Fire 5 (1), 30. http://dx.doi.org/10.3390/fire5010030.

Villaverde, A.F., Pathirana, D., Fröhlich, F., Hasenauer, J., Banga, J.R., 2022. A protocol for dynamic model calibration. Brief. Bioinform. 23, 1–19. http://dx.doi.org/10.1093/bib/bbab387.

Viney, N., 1991. A review of fine fuel moisture modelling. Int. J. Wildland Fire 1 (4), 215–234. http://dx.doi.org/10.1071/WF9910215.

van Wagner, C.E., 1977. A method of computing fine fuel moisture content thought the diurnal cycle. Technical Report, Canadian Forestry Service, URL https://cfs.nrcan.gc.ca/pubwarehouse/pdfs/25591.pdf. accessed: 2 July 2024.

Wang, H., Liang, M., Sun, C., Zhang, G., Xie, L., 2021. Multiple-strategy learning particle swarm optimization for large-scale optimization problems. Complex Intell. Syst. 7, 1–16. http://dx.doi.org/10.1007/s40747-020-00148-1.

Zhang, Y., Sun, P., 2020. Study on the diurnal dynamic changes and prediction models of the moisture contents of two litters. Forests 11 (1), http://dx.doi.org/10.3390/f11010095.